Pergamon

Int. J. Heat Mass Transfer. Vol. 41, No. 15, pp. 2307–2320, 1998

Printed in Great Britain
0017-9310/98 $19.00+0.00

PII: S0017-9310(97)00348-7

On the convection in an enclosed container with unstable side wall temperature distributions

CRAIG C. JAHNKE,† VIKRAM SUBRAMANYAN and DANIEL T. VALENTINE

Mechanical and Aeronautical Engineering Department, Clarkson University, Potsdam, NY 13699-5725, U.S.A.

(*Received* 7 *August* 1997 *and in final form* 3 *November* 1997)

Abstract—A numerical study of natural convection in a two-dimensional container of unity aspect ratio with unstable temperature distributions on the side walls and adiabatic top and bottom walls is discussed for a Boussinesq fluid with unity Prandtl number. For sufficiently low Rayleigh numbers and symmetric boundary conditions a unique 2×2 steady cellular flow with horizontal and vertical symmetry exists. At a critical Rayleigh number a pitchfork bifurcation occurs creating a pair of asymmetric steady solutions. Further increasing the Rayleigh number causes the asymmetric pair of steady solutions to undergo a subcritical Hopf bifurcation resulting in a large amplitude limit cycle. Hysteresis behavior is observed between the stable steady flows and the stable limit cycle for a range of Rayleigh numbers. The limit cycle disappears at a minimum Rayleigh number in what appears to be a double homoclinic orbit. Applying asymmetric temperature boundary conditions causes an unfolding of the pitchfork bifurcation. The character of the Hopf bifurcations and resulting limit cycle behavior is deeply affected by the introduction of asymmetry. As the Rayleigh number is increased a progression of limit cycles containing from two to 206 small amplitude oscillations and one large amplitude 'relaxation' oscillation per period are separated by what may be a series of homoclinic orbits. The steady and limit cycle solution structure has a large influence on the heat transfer rate through the container.

1. INTRODUCTION

Natural convection in an enclosed container has received a great deal of attention by the research community due to its importance in many engineering devices. A particularly important application is the cooling of electronic components in computers. Much of the research has concentrated on the Rayleigh–Bernard problem where the bottom surface of the container is held at a relatively hot temperature, the top surface of the container is held at a relatively cold temperature while the side walls are adiabatic. As the Rayleigh number is increased the flow has been shown to undergo transitions from a state of pure conduction to steady cellular flows, periodic flows, quasi-periodic flows, chaotic flows and ultimately turbulent flow.

Gollub and Benson [1] present experimental results while Curry *et al.* [2] provide numerical results for two- and three-dimensional computations. Various types of instabilities and fluid motions have been found experimentally for Rayleigh–Bernard convection in Hele–Shaw cells [3–6], where the flow is approximately two-dimensional. Steen and coworkers [7–9] have numerically studied these flows, applying continuation techniques to map the steady and oscillatory solutions in parameter space.

A variant of the classic Rayleigh–Bernard problem is obtained by rotating the container 90°. Then one side wall is at a relatively hot temperature, the other side wall is at a relatively cold temperature and the top and bottom of the container are adiabatic. There is no state of pure conduction in this case as a cellular flow develops for any nonzero Rayleigh number. Several types of solutions have been characterized for this flow including steady cellular flows, limit cycles, quasi-period flows, chaos and turbulence [10–12]. The effect of varying inclination angle has also been examined for the Rayleigh–Bernard problem [13].

A related class of flows that has received relatively little attention is that of convection in an enclosed container where unstable temperature distributions are imposed on the side walls while the top and bottom walls are adiabatic [14]. In this class of flows steady multi-cellular convection occurs at low Rayleigh number due to the temperature distributions on the side walls; relatively hot regions of the side walls lead to locally upwelling flows while relatively cold regions lead to locally downwelling flows. Thus, depending on the aspect ratio of the container and the temperature distribution on the side walls any number of cells can be produced.

In this work we consider the case where the upper half of the side walls are relatively cold while the lower

† Author to whom correspondence should be addressed. Tel.: 001 315 268 7687. Fax: 001 315 268 6695. E-mail: craig@sun.soe.clarkson.edu.

half of the side walls are relatively hot leading to a 2×2 steady cellular flow at low Rayleigh numbers. The solution structure of this flow as a function of Rayleigh number is studied numerically through the calculation of steady and limit cycle solutions. For symmetric boundary conditions the solution structure in some ways resembles that found for the Rayleigh–Bernard problem in a Hele–Shaw cell [9]. New results are obtained when the symmetry of the flow is broken by imposing asymmetric boundary conditions. Limit cycle behavior not previously seen in natural convection during which the flow undergoes any number of small amplitude oscillations and one large 'relaxation' oscillation per period is found.

These new limit cycles are symbolically represented as S^mL^n where S represents a small amplitude oscillation, L represents a large amplitude oscillation, m represents the number of small amplitude oscillations, and n the number of large amplitude oscillations per period of the limit cycle. A cascade of S^mL^n type limit cycles where $2 \leqslant m \leqslant 206$ and $n = 1$ is obtained. Limit cycles of the form $(S^3L^1)^i(S^2L^1)^1$ are found to occur in a transition region between S^3L^1 and S^2L^1 type limit cycles. This behavior is related to the existence of multiple unstable steady solutions. The average heat transfer rate through the container is shown to decrease as the flow undergoes transition from stable steady convection to oscillatory convection.

2. EQUATIONS OF FLUID MOTION AND NUMERICAL APPROACH

For the results presented here the flow is assumed to be two dimensional. Additionally the Boussinesq approximation is applied to the fluid such that density variations are linearly related to temperature variations,

$$\rho = \rho_0[1-\alpha_0(T-T_0)] \tag{1}$$

where ρ is the density, T the temperature, and α the coefficient of thermal expansion. The subscript '0' denotes the mean state of the fluid. Then the continuity equation may be written as

$$\frac{\partial u}{\partial x}+\frac{\partial w}{\partial z}=0 \tag{2}$$

the momentum equation as

$$\frac{Du}{Dt}=-\frac{1}{\rho_0}\frac{\partial P}{\partial x}+\nu\nabla^2 u \tag{3}$$

$$\frac{Dw}{Dt}=-\frac{1}{\rho_0}\frac{\partial P}{\partial z}-\alpha_0 g(T-T_0)+\nu\nabla^2 w \tag{4}$$

and the energy equation neglecting frictional heating as

$$\frac{DT}{Dt}=\kappa\nabla^2 T \tag{5}$$

where

$$\frac{D}{Dt}=\frac{\partial}{\partial t}+\left(u\frac{\partial}{\partial x}+w\frac{\partial}{\partial z}\right)$$

$$\nabla^2=\frac{\partial^2}{\partial x^2}+\frac{\partial^2}{\partial z^2}$$

and u and w represent the velocity components in the horizontal, x, and vertical, z, directions, P represents the pressure, ν represents kinematic viscosity, and κ represents thermal diffusivity.

Since the flow is incompressible as regards the continuity equation, one can introduce the stream function, ψ, defined such that

$$u=\frac{\partial\psi}{\partial z},\quad w=-\frac{\partial\psi}{\partial x}$$

which automatically satisfies the continuity equation. The pressure can be eliminated from the momentum equation by combining equation (3) and equation (4) to obtain an equation for the time evolution of the spanwise component of vorticity

$$\frac{D\eta}{Dt}=-Ra\,Pr\frac{\partial\theta}{\partial x}+Pr\,\nabla^2\eta \tag{6}$$

where

$$\eta=\frac{\partial w}{\partial x}-\frac{\partial u}{\partial z}$$

and θ represents the normalized temperature $(T-T_0)/\Delta T$, where ΔT is the difference between the maximum and minimum temperatures at the boundary of the container. Equation (6) has been nondimensionalized using the width of the container, L, as the length scale and the thermal diffusion time scale, L^2/κ, so the Rayleigh and Prandtl numbers are defined as

$$Ra=\frac{g\alpha\Delta TL^3}{\kappa\nu},\quad Pr=\frac{\nu}{\kappa}.$$

The nondimensional form of the energy equation is

$$\frac{D\theta}{Dt}=\nabla^2\theta \tag{7}$$

and the spanwise vorticity can be defined in terms of the stream function as

$$\eta=\nabla^2\psi. \tag{8}$$

Equations (6)–(8) can then be solved for η, θ, and ψ.

No slip and no penetration boundary conditions are imposed on all walls of the container. No penetration is satisfied by defining the stream function to be zero on all bounding surfaces and no slip is imposed through a finite difference approximation to equation (8). Constant temperature distributions are specified

along the side walls of the container, while adiabatic conditions are imposed on the top and bottom walls of the container. The boundary conditions are then

(a) $0 \leqslant x \leqslant 1, \quad z = 0$:

$$\psi = 0, \quad \frac{\partial \theta}{\partial z} = 0, \quad \eta = \left.\frac{\partial^2 \psi}{\partial z^2}\right|_{\frac{\partial \psi}{\partial z} = 0}$$

(b) $x = 0, \quad 0 \leqslant z \leqslant H$:

$$\psi = 0, \quad \theta = \theta_0(z), \quad \eta = \left.\frac{\partial^2 \psi}{\partial x^2}\right|_{\frac{\partial \psi}{\partial x} = 0}$$

(c) $0 \leqslant x \leqslant 1, \quad z = H$:

$$\psi = 0, \quad \frac{\partial \theta}{\partial z} = 0, \quad \eta = \left.\frac{\partial^2 \psi}{\partial z^2}\right|_{\frac{\partial \psi}{\partial z} = 0}$$

(d) $x = 1, \quad 0 \leqslant z \leqslant H$:

$$\psi = 0, \quad \theta = \theta_1(z), \quad \eta = \left.\frac{\partial^2 \psi}{\partial x^2}\right|_{\frac{\partial \psi}{\partial x} = 0}$$

where $\theta_0(z)$ and $\theta_1(z)$ are specified normalized temperature distributions. For the present work $H = 1$ where H is the aspect ratio of the container, defined as the height divided by the width.

Two numerical techniques were applied in the present work. Steady solutions were obtained as a function of Rayleigh number by applying a continuation technique to equations (6)–(8). To perform the continuation calculation the steady versions of equations (6)–(8) were discretized with second-order central differences. The boundary conditions were discretized with second-order one-sided differences where required. A pseudo arc-length continuation technique based on the work of Doedel and Kernevez [15] was then applied to the system of $3NM$ algebraic equations for the discretized approximations to η, θ, and ψ, where N represents the number of grid points in the x-direction and M represents the number of grid points in the z-direction. A steady state was determined to have been reached when both (i) the residual of the discretized forms of equations (6)–(8) and the boundary conditions was less than 10^{-5} at each grid point; and (ii) the maximum relative change of the variables in an iterate at any grid point was less than 10^{-5}.

The second computational technique solved the initial value problem posed by equations (6)–(8). The temporal evolution of η and θ was computed by applying the ETUDE scheme [16] which is a finite difference approximation that is first order in time and nearly second order in space. The Poisson equation, equation (8), was discretized by second-order central differences and solved by successive overrelaxation at each time step for ψ. Numerical accuracy was assured by comparing calculations on uniformly spaced 41×41, 61×61, and 81×81 grids for both numerical methods. Similar results were obtained for all grid sizes. All calculations presented here were performed on an 81×81 uniformly spaced grid and the Prandtl number was equal to 1.0.

3. RESULTS

Temperature boundary conditions on the side walls for both the symmetric and asymmetric cases are shown in Fig. 1. A constant temperature hot wall region in the bottom half of the container is piece-wise linearly connected to a constant temperature cold wall region in the upper half of the container. The linear variation in wall temperature near the half height of the container was used so the boundary condition could be exactly discretized by all computational grids used in this work. Thus, the boundary condition approximates a discontinuity in temperature but avoids the problem that if one has the temperature change occur over only one grid box, then the boundary condition changes as the grid size is varied making it difficult to accurately compare solutions for different grid resolutions. A small region of linear variation is also a more appropriate model for the temperature distribution in a physical device.

Note that the asymmetric boundary condition is only slightly asymmetric, something one might obtain in a carefully built physical device. A certain amount of symmetry is maintained in the asymmetric boundary conditions by reducing the hot region on one side wall and the cold region on the opposite side wall equal amounts. Thus, the boundary conditions maintain a diagonal anti-symmetry which will be evident in most flows.

3.1. *Symmetric boundary condition*

A summary of the steady and limit cycle solutions for the case with symmetric boundary conditions is

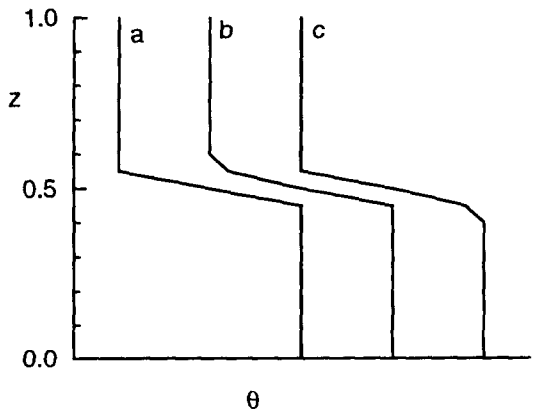

Fig. 1. Temperature boundary conditions on container side walls for (a) symmetric case, $x = 0$, $x = 1$; (b) asymmetric case, $x = 0$; (c) asymmetric case, $x = 1$.

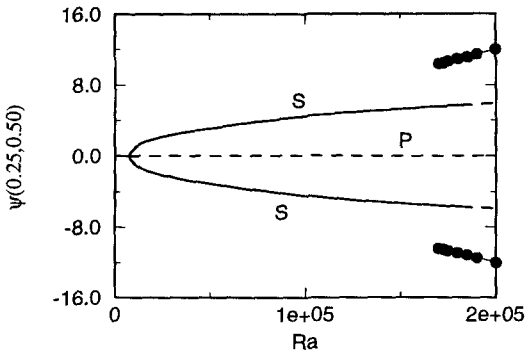

Fig. 2. Bifurcation diagram for symmetric case. Full lines, stable steady solutions; dashed lines, unstable steady solutions; •—maximum and minimum values in stable limit cycles.

shown in the bifurcation diagram of Fig. 2. Steady solutions are represented by the value of the stream function at $(x, z) = (0.25, 0.50)$ while limit cycle solutions are represented by the maximum and minimum values of $\psi(0.25, 0.50)$ in the limit cycle. This variable was chosen so as to present the clearest picture of the results, but any other discretized variable could have been chosen.

As can be seen in Fig. 2, a unique stable steady flow exists for sufficiently small Rayleigh numbers This solution branch will be called the primary solution branch and is labeled P in the figure. Solutions on the primary branch represent 2×2 cellular flows with both vertical and horizontal symmetry about the middle of the enclosure and symmetry about the diagonals of the enclosure. Figure 3 shows a sample of streamline and temperature contours for a solution on the primary branch.

At a critical Rayleigh number near 7915 a pitchfork bifurcation causes the primary branch to become unstable and leads to the emergence of a pair of antisymmetric solutions on a secondary solution branch, labeled S in Fig. 2. Pitchfork bifurcations occur in systems with symmetry and result in new solutions with less symmetry than the original solution. Indeed solutions on the secondary branch do not contain horizontal or vertical symmetry, but the diagonal symmetry is retained. A sample solution on the secondary solution branch is presented in Fig. 4. The secondary branch is characterized by a three cell flow with one large diagonal cell and two smaller corner cells. If the solution along the secondary branch is monitored from the pitchfork bifurcation to larger Rayleigh numbers one sees a gradual merging of two cells along either one of the diagonals (giving the pair of solutions) until a large diagonal cell occurs as shown in Fig. 4.

Secondary solutions are more efficient than primary solutions at transporting heat through the enclosure as shown in Fig. 5 where the heat transfer through the cell, represented by the Nusselt number, is plotted as a function of Rayleigh number. Heat enters the enclosure through the hot portions of the side walls and exits through the cold portions of the side walls. Thus, to enhance heat transfer more hot fluid must be brought near the cold wall and vice versa. Primary solutions have no means of bringing hot fluid near the cold walls by convection, so heat must be conducted from a hot cell to a cold cell and then to the cold wall. The large diagonal cell characteristic of secondary solutions brings hot fluid directly to the cold wall by convection thus improving heat transfer.

As the Rayleigh number is further increased the secondary solutions lose stability in what appears to be a subcritical Hopf bifurcation near $Ra = 180\,000$. For Ra just past the instability, the flow transitions to a large amplitude limit cycle as indicated in Fig. 2. Hysteresis behavior is also evident as stable limit cycles and stable steady flows co-exist for $170\,000 < Ra < 180\,000$.

Figure 6 shows a two-dimensional projection of the phase portrait of the limit cycle for several values of Rayleigh number. The flow oscillates around the three steady solutions, going from one diagonal cell to the other, passing near the primary solution representing the 2×2 cellular array along the way. A sequence of contour plots in the limit cycle for $Ra = 170\,000$ is shown in Fig. 7. As the Rayleigh number is decreased the limit cycle passes closer to the steady primary solution as shown in Fig. 6. Since the flow changes more slowly near a steady solution a disproportionate

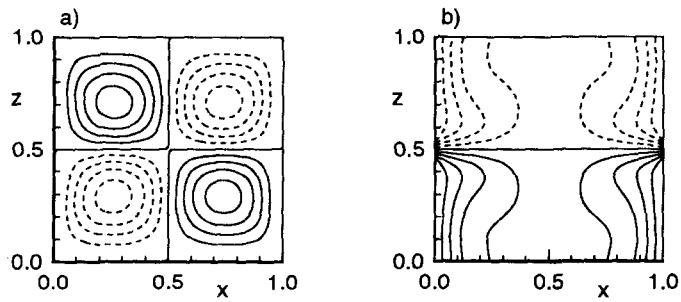

Fig. 3. Contour plots of steady flow on primary solution branch for symmetric case with $Ra = 54\,365$. (a) Streamlines; (b) temperature. Full lines, positive contour levels; dashed lines, negative contour levels.

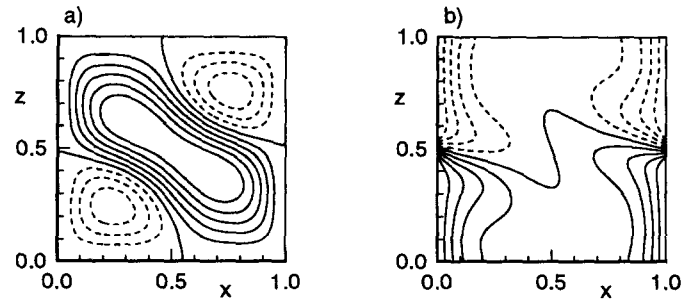

Fig. 4. Contour plots of steady flow on secondary solution branch for symmetric case with $Ra = 54705$. (a) Streamlines; (b) temperature. Full lines, positive contour levels; dashed lines, negative contour levels.

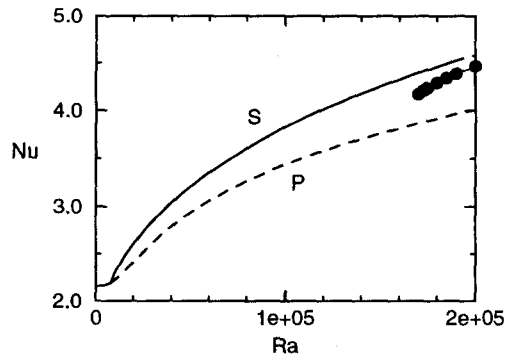

Fig. 5. Time average heat transfer through enclosure for steady and limit cycle solutions as a function of Rayleigh number for symmetric case. Full lines, stable steady solutions; dashed lines, unstable steady solutions; •—stable limit cycles.

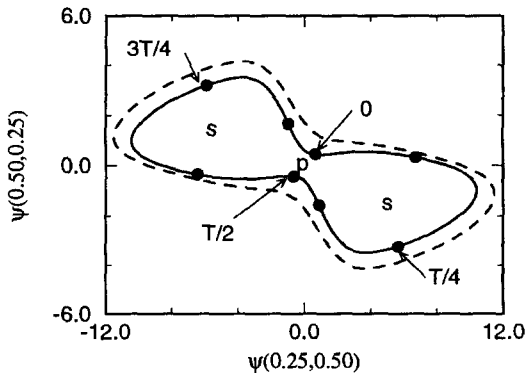

Fig. 6. Projection of phase portrait of limit cycle for symmetric case. Times correspond to contour plots in Fig. 7. Full line, $Ra = 170000$; dashed line, $Ra = 190000$; S—secondary steady solution; P—primary steady solution.

amount of the limit cycle is spent near the primary steady solution. This is evident in Fig. 6 as equal time increments are noted on the limit cycle for $Ra = 170000$. This effect is also evident in the period of the limit cycle which increases as the Rayleigh number is decreased as shown in Fig. 8. This gives the appearance of the limit cycle disappearing at a critical Rayleigh number in a homoclinic bifurcation, but this has not been proven. Qualitatively similar behavior is seen by Hu and Steen [9] for the Rayleigh–Bernard problem in a Hele–Shaw cell.

Since more time in the limit cycle is spent near the primary than the secondary solution, the mean heat transfer through the enclosure is less for the limit cycle solution than for the steady secondary solution as shown in Fig. 5. Indeed the heat transfer rate in the limit cycle is between the heat transfer rate of the primary and secondary solutions as the limit cycle contains remnants of both solutions. Thus, the instability of the secondary solution near $Ra = 180000$ leads to a new stable fluid flow with a reduced heat transfer rate.

3.2. *Asymmetric boundary condition*

Any physical device will have some degree of asymmetry, so it is natural to ask whether the results for symmetric boundary conditions have any relevance to a physical situation. Will a slight asymmetry lead to minor differences from the symmetric flow or will the asymmetric case be qualitatively different? Benjamin [17] has shown that finite aspect ratio Taylor–Couette flow, which is always the case in physical devices, can be quite different from the infinite aspect ratio case that is often treated numerically. For infinite aspect ratio Taylor–Couette flow, a state of purely azimuthal flow exists for low Rayleigh numbers which becomes unstable at a pitchfork bifurcation leading to cellular flows. End walls cause the unfolding of the pitchfork bifurcation resulting in cellular flows at any Rayleigh number.

Since the current problem contains a pitchfork bifurcation for symmetric boundary conditions, we expect an unfolding of the pitchfork bifurcation if any asymmetry is introduced. Asymmetry is provided through the temperature boundary conditions on the side walls as shown in Fig. 1. Note that the asymmetry is minimal, but it has a large effect on the solution structure of the flow as illustrated by the bifurcation diagram in Fig. 9. The pitchfork bifurcation is indeed unfolded leading to a primary steady solution branch, P, that exists for all values of Ra and a pair of steady solutions, SP and SS, that arise at a saddle-node bifur-

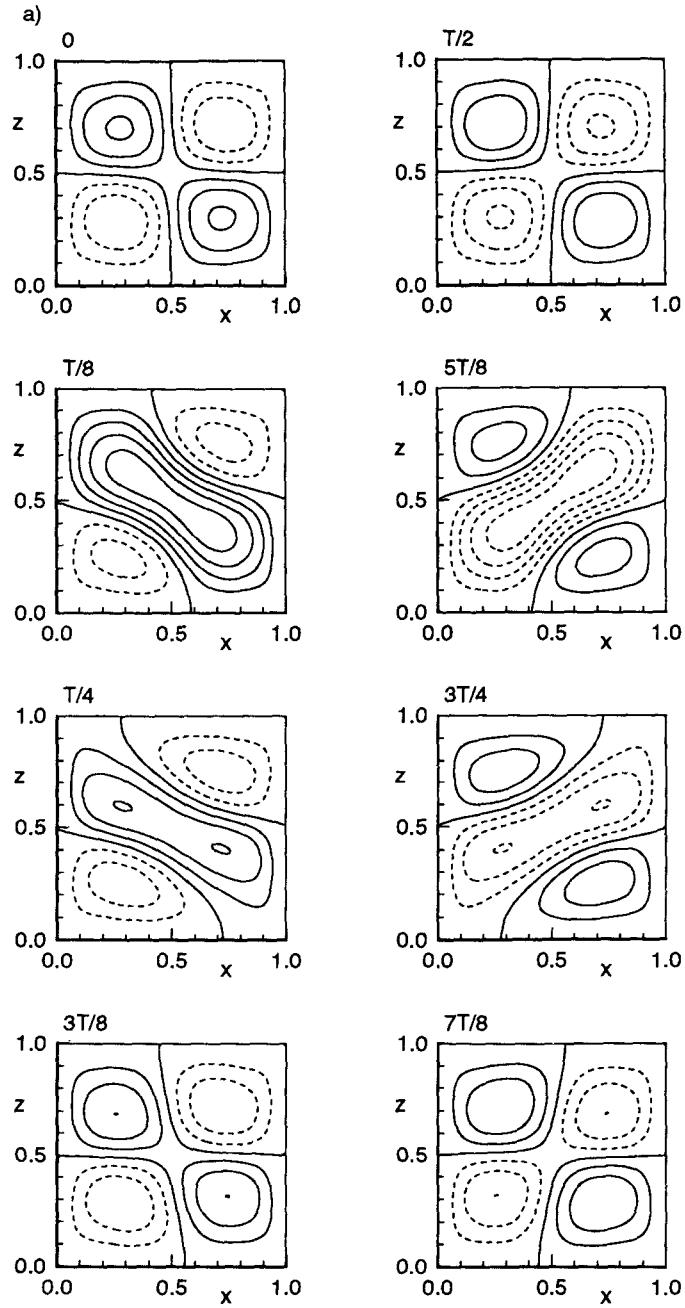

Fig. 7. Contour plots in the limit cycle for symmetric case with $Ra = 170\,000$. (a) Streamlines; (b) temperature. Full lines, positive contour levels; dashed lines, negative contour levels.

cation near $Ra = 12\,990$. Recall that for the symmetric case the pitchfork bifurcation occurred near $Ra = 7915$. An additional pair of steady solutions, PB, arise at a pitchfork bifurcation on the primary branch near $Ra = 286\,135$. This pitchfork bifurcation breaks the diagonal symmetry that exists for solutions on the primary branch.

A sample contour plot of the stream function on each steady solution branch is shown in Fig. 10. Asymmetry is introduced at the left side wall by reducing the region of cold temperature while the region of hot temperature at the right wall is reduced. This favors a flow with more upwelling fluid near the lower left wall and more downwelling fluid near the upper right wall as illustrated by the solution characteristic of the primary branch. Since this flow is favored by the boundary conditions, it remains stable to a higher Rayleigh number, $Ra = 247\,000$, than branch SS which loses stability near $Ra = 136\,000$. Branch SP solutions are similar to the 2×2 cellular flow on the primary branch

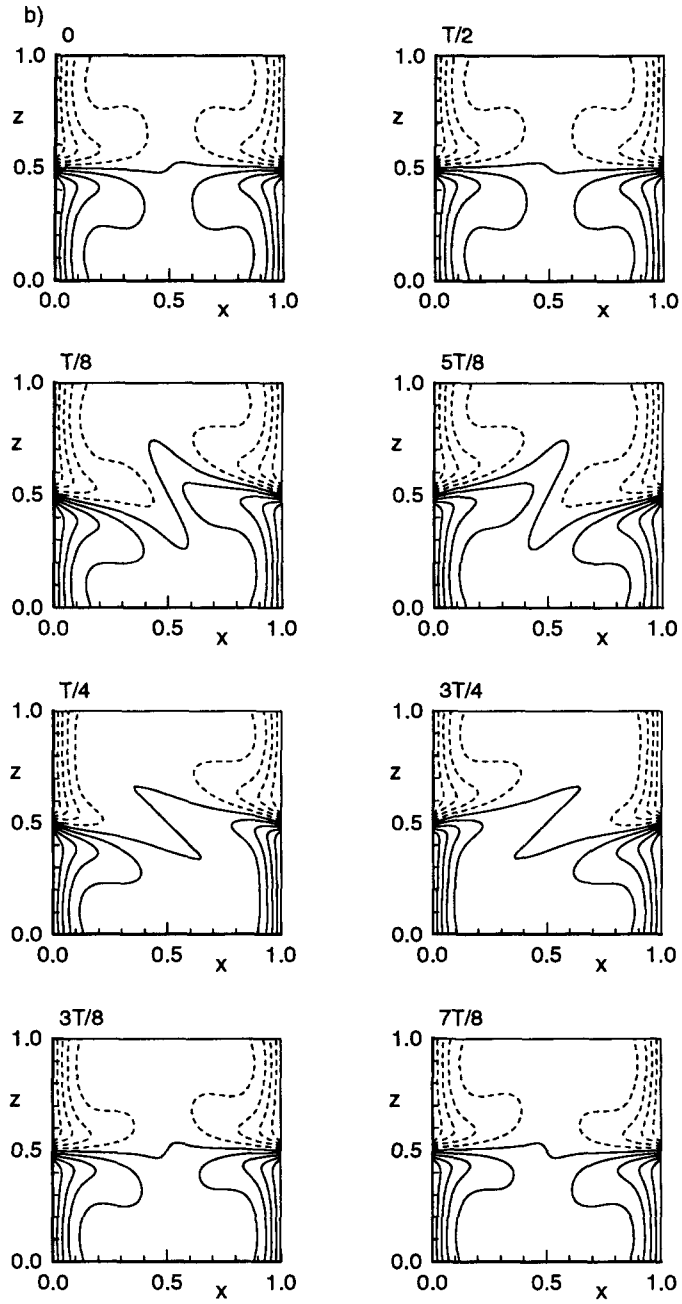

Fig. 7—*continued.*

for the symmetric case due to the small amount of asymmetry. Solutions on branch PB do not have the diagonal symmetry that solutions on branches P, SS, and SP contain. While solutions on branch PB are always unstable, and thus would not be seen to occur experimentally, the pitchfork bifurcation from which they arise breaks the diagonal symmetry and could influence the flow. Recall that the unstable steady solutions had a large effect on the limit cycle behavior for the symmetric case.

Branch SS becomes unstable at $Ra = 136\,000$ due to what appears to be a subcritical Hopf bifurcation. Just past the critical Rayleigh number at which branch SS becomes unstable no stable limit cycle is found. For time simulations starting from an unstable steady solution on branch SS growing oscillations occur with the flow eventually transitioning to a stable steady solution on the primary solution branch.

Stable limit cycles occur when the primary solution branch becomes unstable at a supercritical Hopf bifurcation near $Ra = 247\,000$ (see Fig. 9). Small amplitude limit cycles that represent the flow oscillating about

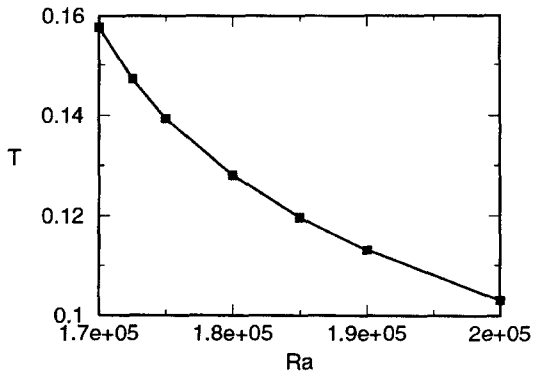

Fig. 8. Period of limit cycle as a function of Rayleigh number.

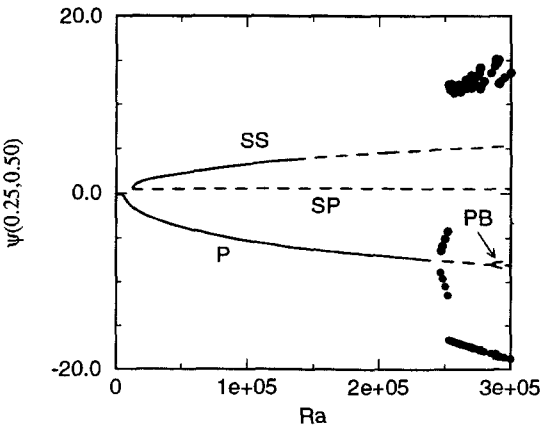

Fig. 9. Bifurcation diagram for asymmetric case. Full lines, stable steady solutions; dashed lines, unstable steady solutions; •—maximum and minimum values in stable limit cycles.

the primary steady solution occur for $247\,000 \leqslant Ra \leqslant 252\,000$. Between a Rayleigh number of 252 000 and 253 000 the small amplitude limit cycles lose stability in what may be a heteroclinic bifurcation. This conjecture is based on numerical simulations and examination of the resulting two dimensional projections of phase space, so it is far from proven. What is observed is that for $Ra = 252\,000$ a time simulation started at the primary steady solution shows that the flow very slowly approaches a small amplitude limit cycle. For $Ra = 253\,000$ the flow is initially attracted to a small amplitude limit cycle, but eventually spirals away and undergoes limit cycle behavior that combines both small and large amplitude oscillations.

Regardless of the details of the instability of the small amplitude limit cycle the flow behavior for Rayleigh numbers larger than 253 000 is quite different from that seen for smaller Rayleigh numbers and for the symmetric case. An example of this limit cycle behavior is presented in Fig. 11 for $Ra = 292\,000$ through a two-dimensional projection of phase space and a time trace of the value of the stream function at one location in the flow. The time trace shows that a sequence of two small amplitude oscillations occurs for every large amplitude oscillation. This type of limit cycle has been seen in reaction-diffusion systems where it is related to the existence of a 'spiraling out' homoclinic orbit of Sil'nikov type [18]. Limit cycles with combinations of small and large amplitude oscillations can be described symbolically as S^mL^n, where S^m represents m small amplitude oscillations and L^n represents n large amplitude 'relaxation' oscillations. Using this notation the limit cycle for $Ra = 292\,000$ is of the type S^2L^1.

As can be deduced from the phase plot of Fig. 11 the flow is oscillating about the steady solutions P, SP and SS. Since the asymmetry of the problem favors a flow structure represented by the primary steady solution (i.e. this steady solution is least unstable) more time is spent in the vicinity of P. Just as in the symmetric case, the steady solutions (even though they are unstable) have a strong influence on the limit cycle behavior. Figure 12 presents a sequence of contour plots in the limit cycle at $Ra = 292\,000$. The flow oscillates between cellular flows qualitatively similar to the steady flows P and SS (see Fig. 10). Note that the large diagonal cell evident in the streamline contour plots does not rotate in transitioning from one orientation to the next. There is a pinching off of the large cell and a reconnection of the two smaller cells in the process.

A sequence of limit cycles of the form S^mL^n occurs for $253\,000 \leqslant Ra \leqslant 300\,000$, where $2 \leqslant m \leqslant 206$ and $n = 1$. A summary of these solutions is given in Table 1. The maximum number of small oscillations per limit cycle was found for $Ra = 253\,000$. This is the value of Ra nearest to the value where the small amplitude limit cycle becomes unstable. Thus, the system is initially attracted toward the small amplitude limit cycle, but since the limit cycle is slightly unstable slowly growing oscillations occur until the system undergoes one large amplitude oscillation and repeats the cycle. The small amplitude oscillations grow slower if the small amplitude limit cycle is less unstable leading to more small oscillations per large amplitude oscillation. In the limit of the small amplitude limit cycle becoming neutrally stable an infinite number of small amplitude oscillations per large amplitude oscillation would occur leading to a limit cycle with infinite period. This trend is evident in Fig. 13 which shows the period of the limit cycles as a function of Rayleigh number. Note that the period of the limit cycle for $Ra = 253\,000$ ($T \approx 9.05$) is off the scale of the plot.

The period of the S^mL^n type limit cycle is a piecewise continuous function of Rayleigh number. Jumps in the period occur when the flow transitions from a S^mL^1 to a $S^{m+1}L^1$ limit cycle. This discontinuous transition explains the behavior of the maximum amplitude of the stream function in the limit cycle seen in Fig. 9. Insight into why the flow makes a sudden transition from a S^mL^1 to a $S^{m+1}L^1$ limit cycle can be obtained

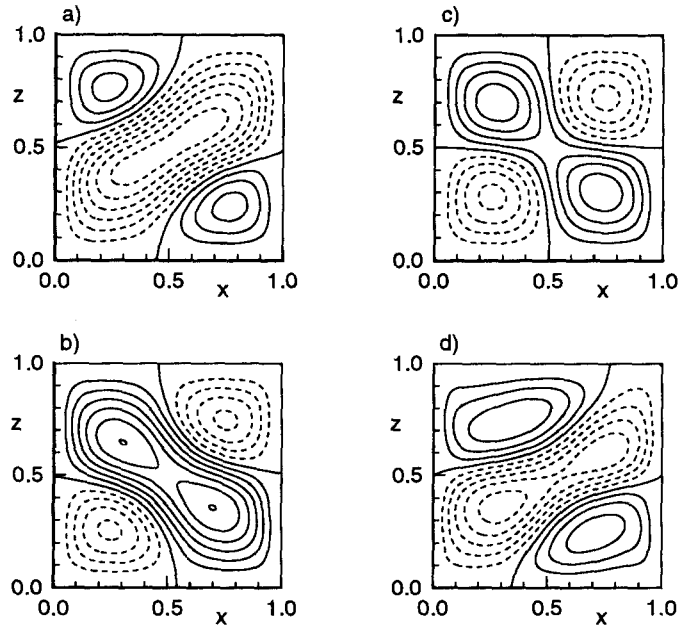

Fig. 10. Contour plots of the stream function on the steady solution branches for the asymmetric case. (a) Branch P, $Ra = 53\,268$; (b) branch SS, $Ra = 58\,930$; (c) branch SP, $Ra = 53\,087$; (d) branch PB, $Ra = 350\,206$. Full lines, positive contour levels; dashed lines, negative contour levels.

by comparing phase plots for several different limit cycles. Figure 14 shows phase plots for the S^5L^1 limit cycle at $Ra = 270\,000$ and the S^4L^1 limit cycle at $Ra = 270\,500$. The growing spirals in the phase plot represent the small amplitude oscillations while the large loop represents the large amplitude oscillation. Growing small amplitude oscillations can persist as long as they stay to the left of the steady solution SP, once a spiral goes to the right of SP a large amplitude oscillation occurs.

Now consider what happens as the Rayleigh number is increased from 270 000–270 500. The growth rate of the spirals increases as the Rayleigh number increases, so in a given number of oscillations the state of the system gets closer to SP. At a critical Rayleigh number between 270 000 and 270 500, the spiral's growth rate is large enough such that the fifth spiral goes to the right of SP instead of the left and transitions to the S^4L^1 limit cycle. A discontinuity arises as the flow must decide whether to go to the left or the right of SP; it has either four or five small amplitude oscillations per limit cycle. It is possible that a homoclinic orbit exists at the critical Rayleigh number between a S^mL^1 and $S^{m+1}L^1$ limit cycle but this has not been proven. Proving that a homoclinic orbit exists is a formidable task for such a complicated problem.

Attempting to resolve the transition between the S^3L^1 and S^2L^1 limit cycles led to the discovery of a sequence of limit cycles of the form $(S^3L^1)^i(S^2L^1)$ where i varied from 1 to 17 as listed in Table 2. Figure 15 shows samples of $(S^3L^1)^1(S^2L^1)$ and $(S^3L^1)^4(S^2L^1)$ limit cycles. This type of limit cycle explains the large periods for limit cycles near $Ra = 289\,000$ in Fig. 13. This new sequence of limit cycles leads one to wonder whether there exists another sequence between the $(S^3L^1)^{i+1}(S^2L^1)$ and $(S^3L^1)^i(S^2L^1)$ type limit cycles; none has been found to date. Part of the reason for this may be that time simulations are an inefficient means of finding limit cycles due to the length of simulations required. This is only exacerbated by the very long periods of the $(S^3L^1)^i(S^2L^1)$ type limit cycles.

The transition between S^4L^1 and S^3L^1 type limit cycles was also examined by performing time simulations around the critical Rayleigh number but no $(S^4L^1)^i(S^3L^1)$ type limit cycle behavior was observed. The critical Rayleigh number was resolved to be between 276 595 and 276 596, so either no $(S^4L^1)^i(S^3L^1)$ type limit cycles exist or they occur in such a narrow region that we cannot reasonably hope to find them with time simulations. Note that the Rayleigh number range for which a S^mL^1 type limit cycle exists decreases as m increases, so one would expect the transition from $S^{m+1}L^1$ to S^mL^1 limit cycles to also occur in a smaller range of Rayleigh numbers for larger values of m.

As shown in Fig. 16, the mean heat transfer through the enclosure is less for limit cycle solutions than for the steady primary solution. In the limit cycle, the general features of the flow oscillate between those representative of the P, SS, and SP steady solutions, so it is not surprising that the average heat transfer in the limit cycle is between that of the various steady solutions. Transitions from one type of limit cycle to another are evident in the heat transfer rate for Rayleigh numbers near 276 000 and 290 000. Recall that for a Rayleigh number near the transition value, the

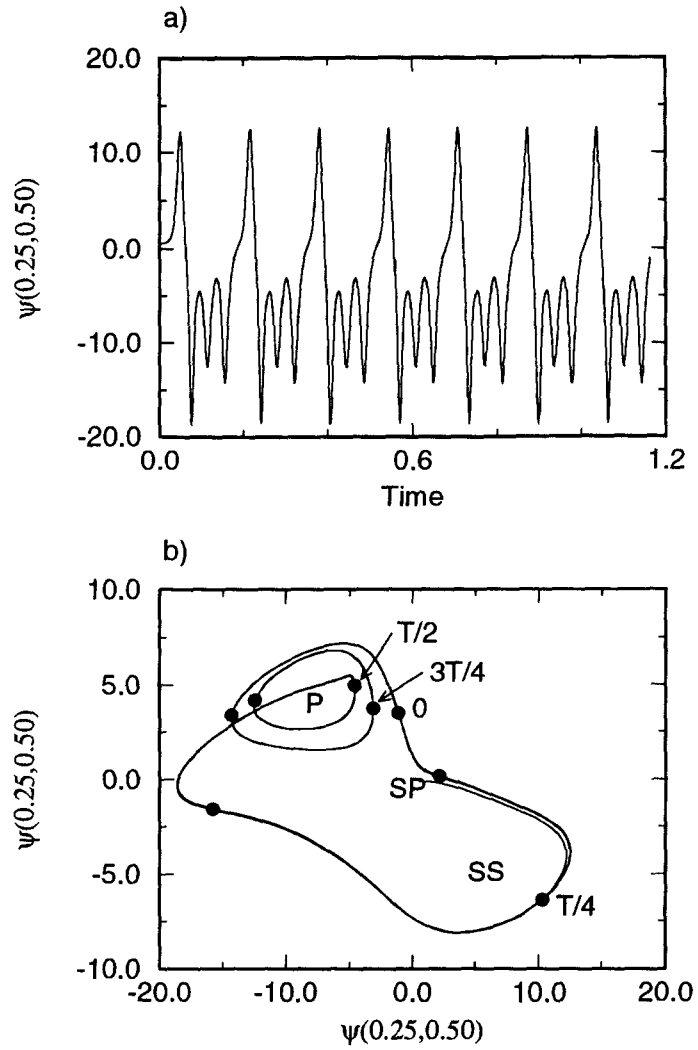

Fig. 11. Time simulation for asymmetric case with $Ra = 292\,000$. (a) Time series; (b) two-dimensional projection of phase space; SS, SP, P—location of corresponding steady solutions; •—equally increments of time at which contour plots are obtained in Fig. 12.

limit cycle comes very close to the steady solution on branch SP (see Fig. 14) and spends a disproportionate amount of time in the vicinity of this steady solution. Since the heat transfer rate is low for steady solutions on branch SP, the more time the limit cycle spends in the vicinity of SP the lower the average heat transfer rate. This accounts for the local dips in the heat transfer rate near Rayleigh numbers of 276 000 and 290 000, where the transitions between limit cycle types is well resolved.

4. SUMMARY AND DISCUSSION

The temperature boundary conditions examined in this study produced a buoyancy induced flow where at sufficiently low Rayleigh numbers the flow exhibits a steady 2×2 cellular pattern. At a critical Rayleigh number a pitchfork bifurcation occurs breaking the symmetry of the flow, while a Hopf bifurcation leads to oscillatory flows at higher Rayleigh numbers. A homoclinic orbit is also suggested to occur producing a solution structure with qualitative similarities to that seen by Hu and Steen [9] for Rayleigh–Bernard convection in a tall Hele–Shaw cell.

Numerical studies often impose symmetry conditions on the flow domain and/or the boundary conditions and neglect to consider the effects of small asymmetries that would be present in a physical device. Since pitchfork bifurcations only occur in systems with some degree of symmetry it is not possible to find pitchfork bifurcations in physical devices where unavoidable asymmetries lead to an unfolding of the pitchfork bifurcation. As shown by the present results,

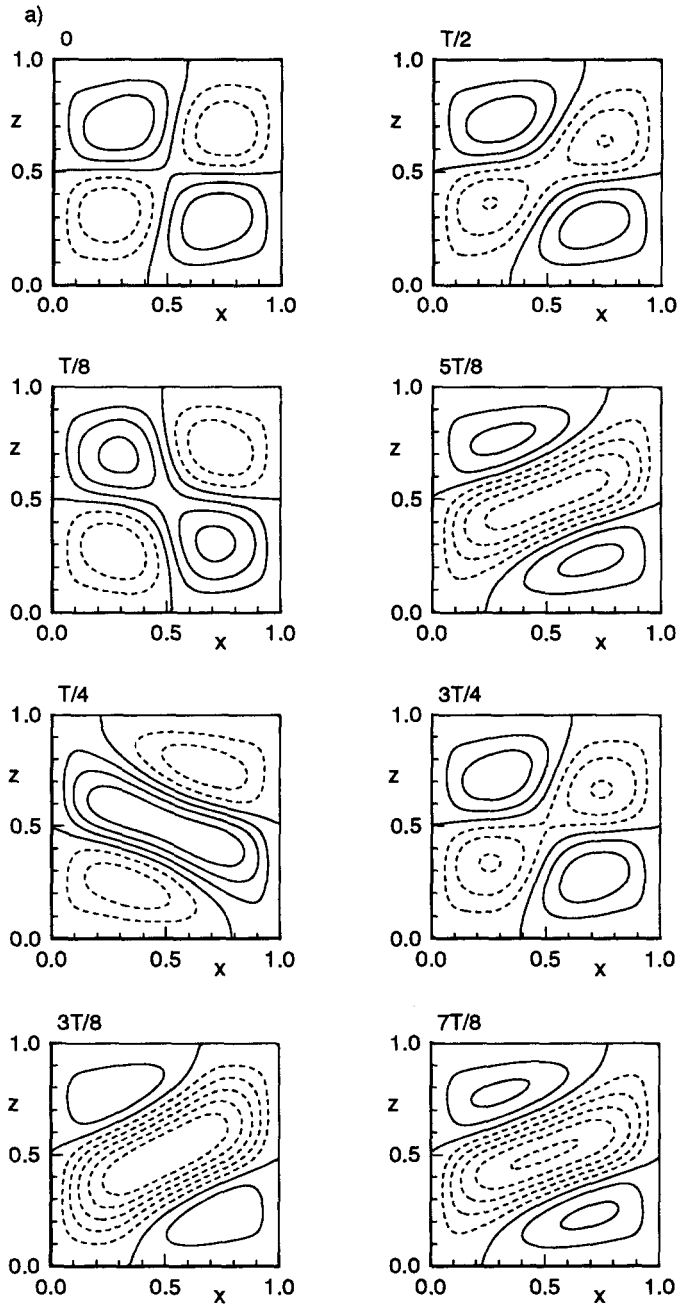

Fig. 12. Contour plots in the limit cycle for an asymmetric case with $Ra = 292\,000$. (a) Streamlines; (b) temperature. Full lines, positive contour levels; dashed lines, negative contour levels.

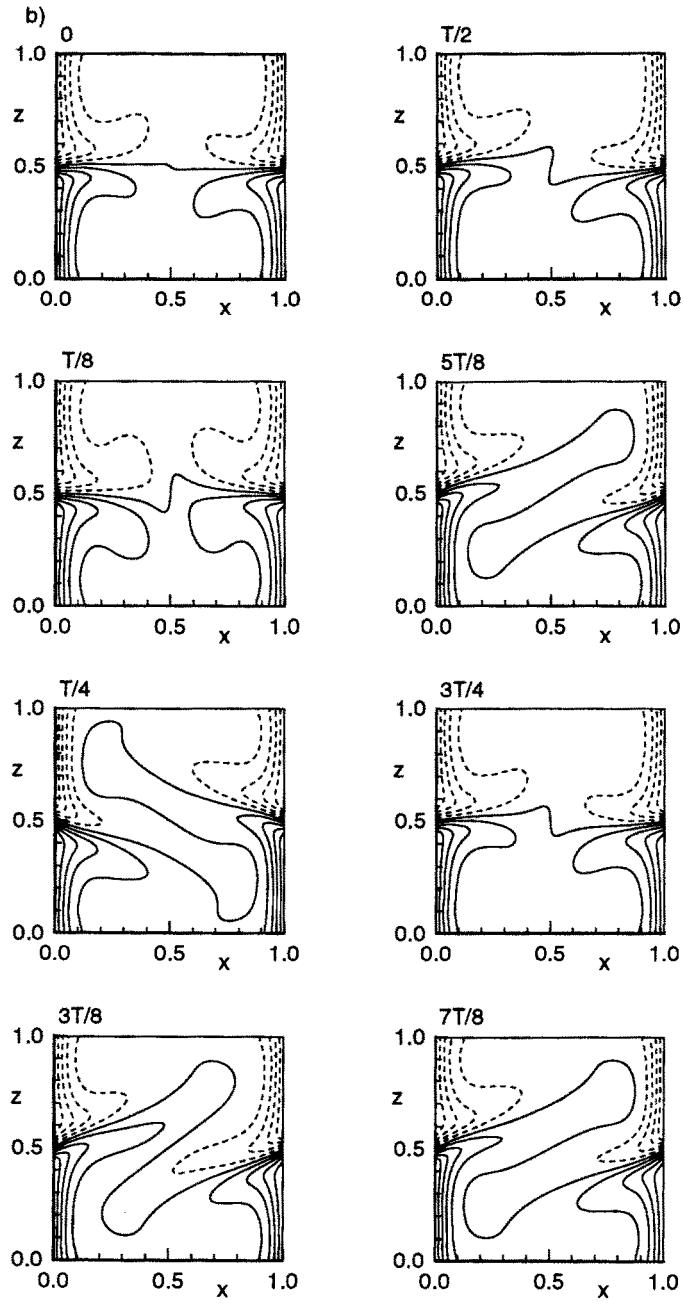

Fig. 12—*continued.*

Table 1. S^mL^1 type limit cycles

Rayleigh number	m
253 000	206
254 000	39
255 000	25
255 000	21
256 000	18
256 500	16
257 000	14
257 500	13
258 000	12
258 500	11
259 000	10
260 000 → 260 500	9
261 000 → 261 500	8
262 000 → 263 000	7
264 000 → 266 000	6
266 750 → 270 000	5
270 500 → 276 595	4
276 596 → 288 600	3
291 250 → 300 000	2

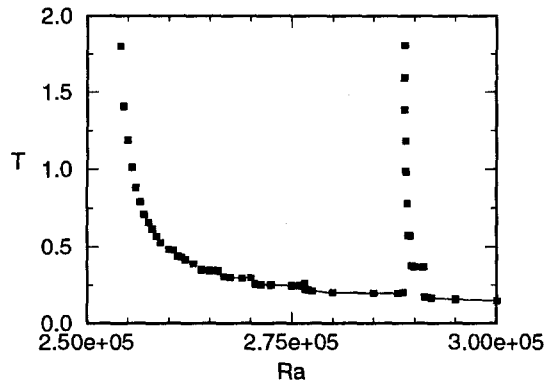

Fig. 13. Period of S^mL^1 type limit cycles as a function of Rayleigh number for the asymmetric case.

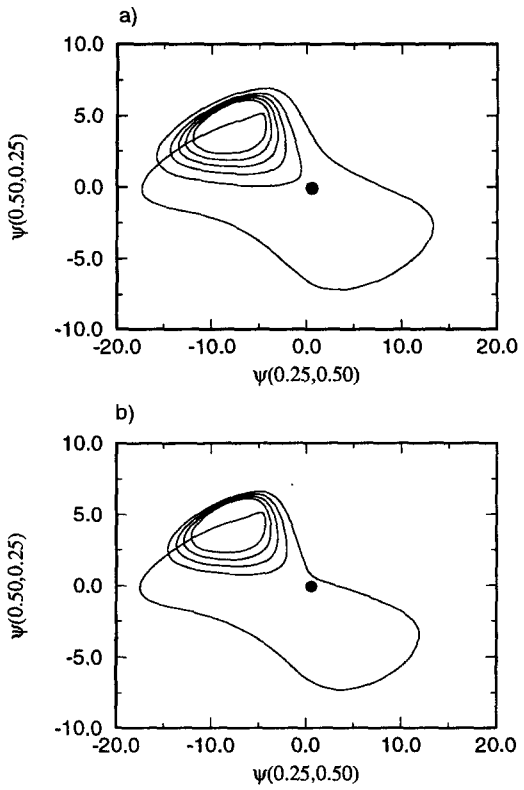

Fig. 14. Time simulation for asymmetric case with (a) $Ra = 270\,000$, S^5L^1 limit cycle; (b) $Ra = 270\,500$, S^4L^1 limit cycle. ●—SP steady solution.

Table 2. $(S^3L^1)^i(S^2L^1)$ type limit cycles

Rayleigh number	i
288 650	17
288 700	10
288 725	9
288 750	8
288 775	7
288 800	6
288 875	5
288 900 → 289 000	4
289 100	3
289 250 → 289 500	2
289 700 → 291 200	1

a small asymmetry can have major effects on the flow behavior. Critical Rayleigh numbers at which bifurcations occur and the types of bifurcations change when asymmetry is introduced. New limit cycle behavior is also observed as a result of the differing degrees of instability of the steady solutions due to the introduced asymmetry.

The approach of first calculating the steady solutions and their stability so as to help interpret the subsequent time simulations was shown to be very effective. Unstable steady solutions were found to affect the characteristics of the limit cycle solutions and knowledge of the steady solutions benefited our interpretation of the flow physics. Continuation techniques are very useful in that stable and unstable solutions are determined, unlike time simulations which only produce steady solutions. Ideally one would also like to determine the limit cycle solutions as a function of the system parameters with a continuation technique, as done by Hu and Steen [9], but the computational requirements for this are beyond our current resources. The question of whether a low dimensional dynamical system can model the complex dynamics of this flow is also an intriguing issue for future study.

Acknowledgements—Partial funding for this work was provided by the National Science Foundation under Grant Number CMS-9409025 and the National Aeronautics and Space Administration under Grant Number OSP-5039.

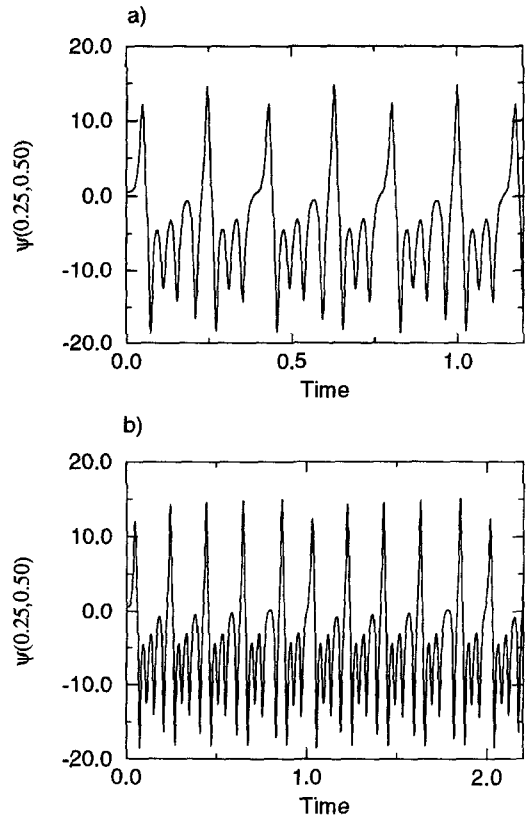

Fig. 15. Time simulation for asymmetric case with (a) $Ra = 289\,700$, $(S^3L^1)^1(S^2L^1)$ limit cycle; (b) $Ra = 289\,000$, $(S^3L^1)^4(S^2L^1)$ limit cycle.

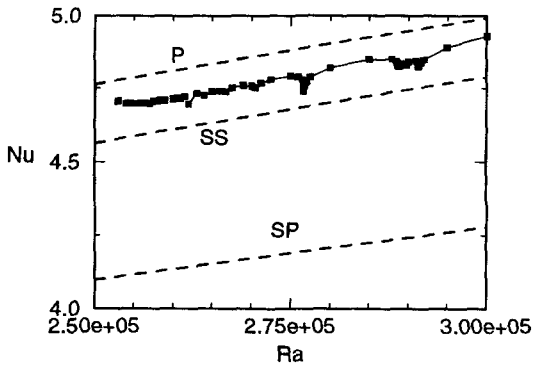

Fig. 16. Time average heat transfer through enclosure for steady and limit cycle solutions as a function of Rayleigh number for asymmetric case.

REFERENCES

1. Gollub, J. P. and Benson, S. V., Many routes to turbulent convection. *Journal of Fluid Mechanics*, 1980, **100,** 449–470.
2. Curry, J. H., Herring, J. R., Loncaric, J. and Orsag, S. A., Order and disorder in two- and three-dimensional Bernard convection. *Journal of Fluid Mechanics*, 1984, **147,** 1–38.
3. Koster, J. N., Interaction of local instabilities during oscillatory convection. *Physical Review A*, 1988, **37,** 3410–3422.
4. Koster, J. N. and Muller, U., Free convection in vertical gaps. *Journal of Fluid Mechanics*, 1982, **125,** 429–451.
5. Koster, J. N. and Muller, U., Oscillatory convection in vertical slots. *Journal of Fluid Mechanics*, 1984, **139,** 363–390.
6. Frick, H. and Muller, U., Oscillatory Hele–Shaw convection. *Journal of Fluid Mechanics*, 1983, **126,** 521–532.
7. Graham, M. D., Muller, U. and Steen, P. H., Time-periodic thermal convection in Hele–Shaw slots: the diagonal oscillation. *Physics of Fluids A*, 1992, **4,** 2382–2393.
8. Graham, M. D. and Steen, P. H., Plume formation and resonant bifurcations in porous-media convection. *Journal of Fluid Mechanics*, 1994, **272,** 67–89.
9. Hu, W. and Steen, P. H., Transition to chaotic natural convections in tall Hele–Shaw slots. *Physics of Fluids*, 1996, **8,** 1929–1937.
10. Chenoweth, D. R. and Paolucci, S., Natural convection in an enclosed vertical air layer with large horizontal temperature differences. *Journal of Fluid Mechanics*, 1986, **169,** 173–210.
11. Paolucci, S. and Chenoweth, D. R., Transition to chaos in a differentially heated vertical cavity. *Journal of Fluid Mechanics*, 1989, **201,** 379–410.
12. LeQuere, P., A Note on multiple and unsteady solutions in two-dimensional convection in a tall cavity. *Journal of Heat Transfer*, 1990, **112,** 965.
13. Hart, J. E., Stability of the flow in a differentially heated inclined box. *Journal of Fluid Mechanics*, 1971, **47,** 547–576.
14. Poulikakos, D., Natural convection in a confined fluid-filled space driven by a single vertical wall with warm and cold regions. *Journal of Heat Transfer*, 1985, **107,** 867.
15. Doedel, E. J. and Kernevez, J. P., Software for continuation problems in ordinary differential equations with applications. Preprint, California Institute of Technology, 1985.
16. Valentine, D. T., Decay of confined, two-dimensional, spatially periodic arrays of vortices: a numerical investigation. *International Journal of Numerical Methods in Fluids*, 1995, **21,** 155.
17. Benjamin, T. B., Bifurcation phenomena in steady flows of a viscous fluid I. Theory. *Proceedings of the Royal Society of London A*, 1978, **359,** 1–26.
18. Arnéodo, A., Argoul, F., Elezgaray, J. and Richetti, P., Homoclinic chaos in chemical systems. *Physica D*, 1993, **62,** 134–169.